Multivariable compensation of hysteresis, creep, badly damped vibration and cross-couplings in multi-axes piezoelectric actuators

Didace HABINEZA, Mahmoud ZOUARI, Yann LE GORREC, *Member, IEEE*
and Micky RAKOTONDRABE*,*Member, IEEE*

Abstract— **This paper presents the control of a two degrees of freedom (2-DOF) piezoelectric actuator that exhibits hysteresis nonlinearity, creep nonlinearity, badly damped vibration and cross-couplings without using feedback sensors. The principle consists in compensating first the hysteresis, then the creep and finally the vibration. The proposed compensation technique is multivariable and therefore is also able to reduce the cross-couplings which are unwanted phenomena. The experimental tests demonstrate that the hysteresis which initially exceeds 19% is reduced to about 0.01% while the creep is reduced from 5.5% to 0.04%. Regarding the vibration, the related overshoot which was initially 45% is completely removed.**

Note to Practitioners **This paper describes an approach to control and to automate dexterous precise positioning systems based on multi-axes piezoelectric actuators. Two problems have motivated the approach investigated in the paper: i) the presence of nonlinearities (hysteresis and creep), of badly damped vibration and of cross-couplings in the multi-axes piezoelectric actuators, ii) and the lack of convenient sensors to feedback control them. Therefore, this paper proposes multivariable and complete feedforward control approach that does not require external sensors. This sensor-less control architecture permits a low cost and a high integration features additionally to the fact that it is of great interest in applications at small scales where implementation of real-time measurement system is often difficult.**

Index Terms— **Multi-DOF piezoactuators, multivariable modeling, multivariable feedforward control, hysteresis, creep, badly-damped vibration, cross-couplings.**

I. INTRODUCTION

Piezoelectric actuators (PEA) rank among the most used actuators in micro/nano-applications. Their notoriety is thanks to their high bandwidth, high resolution, high stiffness and high force generation, rapidity of the response (high operating bandwidth) and the ease of integration in micro/nano-systems. From the operational point of view, most of PEA can be categorized into two main groups. The first group includes all mono-axis piezoelectric actuators. These actuators are made to provide displacements along one direction. Among them we can name piezostacks and piezocantilevers, these latters being very used in micro/nano-assembly and manipulation tasks.

The second group includes actuators able to provide displacements along several axes. Piezostages and piezoelectric tubes (piezotubes) are among these actuators. They are mainly used for spatial positioning tasks, such as scanning microscopy. However, PEA are also known to exhibit unwanted phenomena that compromise the overall performances of the tasks, such as their precision or even their stability. These phenomena are principally the hysteresis nonlinearity, the creep nonlinearity and the badly damped vibration that appears when a PEA is excited with a brusque input voltage. To counterbalance these phenomena, control of the PEA is essential.

The control of PEA has raised many works available in the literature. Their objectives are to reduce the nonlinearities and the vibration that typify the actuators in order to reach some desired tasks performances. The most used strategies are based on feedback architecture which permits to ensure robustness against eventual external disturbances or against model uncertainties [1]–[9]. Though these strategies offer very interesting performances, they are not usually implementable for small scales piezoelectric systems. In fact, there is a lack of convenient sensors at these scales such that the implementation of feedback control architecture is often impossible [1], [10]. Indeed, sensors capable of furnishing the required bandwidth and resolution to measure the piezoelectic actuators performances are bulky and expensive, examples include optical triangulation based sensors, camera based measurement and interfermetry based sensors. Even if they are employable in laboratory experiences, they cannot be used in batch produced systems because of the cost. Furthermore, due to their sizes, they are not convenient for measuring the displacements of multi-axes systems. In counterpart, sensors that can be embedded easily (strain gage, capacitive...) are limited in performances, mainly in term of signal-to-noise ratio, range of measurement and bandwidth. An alternative way to using external sensors consists in using the piezoelectric actuator as its proper sensor by exploiting simultaneously the direct and the converse piezoelectic effects. This approach is called self-sensing approach and has been initially developed for vibration damping [11]–[17]. Due to the charge leakage within the piezoelectric actuator, self-sensing could not be used when the displacement or force is constant or at low frequency. However, by modeling the leakage and by compensating it thanks to an algorthim, static and dynamic self-sensing has been made possible [18], [19].

Another interesting alternative to external sensors based

control is the open-loop control. It is an architecture that does not require sensors at all. Open-loop or feedforward control architecture for piezoelectic actuators has been extensively studied and applied because of its low-cost and high integration features (no external sensors required). Roughly speaking, the principle consists in modeling as precise as possible the unwanted phenomenon (hysteresis, creep or badly damped vibration) and then employing the inverse or the approximate inverse of the model as compensator by cascading this latter with the process.

There are abundant works in the literature regarding the feedforward control of hysteresis nonlinearity in PEA. Among them, the Prandtl-Ishlinskii [20]–[27], the Preisach [28]–[32], and the Bouc-Wen [33] approaches have been developed and implemented. Regarding the modeling and feedforward control of creep nonlinearity, techniques based on logarithmic equations [34] and based on linear time invariant (LTI) models [35] have been used. Finally, regarding the feedforward control of the vibration in PEA, principal approaches employ a LTI model combined with input shaping techniques [36], [37], or with open-loop H_∞ technique [38]. All these feedforward control works dealt however with the compensation of one phenomenon only, i.e. either the hysteresis, the creep or the vibration. In [39], [40], the feedforward control of both the hysteresis and the creep has been carried out while in [41], the vibration and the hysteresis have been treated. The modeling and compensation of the three phenomena (hysteresis, creep and vibration) simultaneously have first been suggested in [42] where the application was the images scanning with an atomic force microscopy. The principle consisted in considering them as three phenomena in cascade. The global compensator was also a cascade of the individual compensators. Later on [35], [43], the same cascade architecture has been used but with other techniques for the individual models and compensators.

Additionally to the hysteresis, to the creep and to the vibration, cross-couplings are phenomena that cause loss of accuracy in tasks performed by PEA. In fact cross-couplings are found in muti-axes PEA and are observed as the apparition of unwanted displacements in the other axes when one axis is excited. Cross-couplings can be caused by a misalignment of the electrodes in the PEA, by a mechanical design defect, or by the misalignment of the sensors axes relative to the PEA axes. The two former causes are the most delicate because only control can reduce or minimize their consequences if the initial design could not be anymore improved. To this aim, feedback control of multi-axes PEA has been studied and has resulted in very good performances [44]–[47]. But, again the lack of convenient sensors makes this architecture less used or even difficult to implement for small scales applications. On the other hand, feedforward control of multi-axes PEA has been studied in order to compensate for the multivariable hysteresis and related cross-couplings [48], [49], or to compensate for the multivariable creep and related cross-couplings [50], or again to compensate for the multivariable vibration and related cross-couplings [51]–[53]. These techniques perform the compensation of the phenomena in an individual manner and not simultaneously. However, all the phenomena (hysteresis, creep, vibration and cross-couplings) occur simultaneously when the multi-axes PEA should work at static (low frequency) and at dynamic (high frequency) conditions to effectuate high precision and high bandwidth tasks. Compensating them within the same controller is therefore vital.

Relative to the above mentionned works, this paper suggests to simultaneously control the hysteresis, the creep, the vibration and the cross-couplings in multi-axes piezoelectic actuators. Called complete compensation, the control of the four phenomena is performed without using external sensors which makes the approach very valuable for PEA based positioning systems at small scales. To this aim, the approach consists in cascading three multivariable compensators which are: a compensator for the hysteresis, a compensator for the creep and a compensator for the vibration. Since the three compensators are designed to be multivariable, they automatically account for the cross-couplings. Regarding the hysteresis, the model and the compensator are based on the Bouc-Wen technique. On the other hand, we suggest to tackle the creep and the vibration with multivariable LTI (linear time invariant) models. The different compensators are such that direct inversion of models is avoided, and thus models invertibility condition is not necessary. This makes the derivation and calculation of the suggested compensators simple. The experiments are carried out on a two degrees of freedom (2-DOF) piezotube actuator classically used in atomic force microscopy and in precise positioning. The results demonstrate the efficiency of the complete compensator to compensate for all the unwanted phenomena.

The paper is organized as follows. In section-II we first present the experimental setup and the PEA. In section-III we give the general principle and the procedure of the compensation approach. Section-IV is devoted to the compensation of the multivariable hysteresis. In section-V the compensation of the multivariable creep is detailed and added to the previous hysteresis compensation. Section-VI is devoted to the complete compensation by introducing the vibration compensator to the previous hysteresis and creep compensators. The different compensators are multivariable and thus can handle the cross-couplings. Finally, we give some discussions in section-VII and conclusions and perspectives in section-VIII.

II. PRESENTATION OF THE EXPERIMENTAL SETUP

In this scetion, we present the experimental setup. The main core of the experimental setup is a piezoelectic actuator (PEA). Both the models and the compensators (feedforward controllers) will be studied from this PEA.

A. The piezotube actuator

The PEA used is a piezotube (PT 230.94 fabricated by *Physik Instrumente* company). This actuator has a tubular structure and is made of PZT (lead zirconate titanate) material coated by four external electrodes +x, -x, +y and -y, and one inner electrode that serves as ground (Fig. 1a). When an electrical potential $+u$ is applied to one electrode and its opposite $-u$ is applied to the antagonist electrode, we obtain an expansion and a contraction respectively of the

two antagonist sectors of the tube. This results in an overall deflection, and thus a displacement, along x axis or along y axis according to which pair of electrodes is supplied (Fig. 1b upper). When the four external electrodes are supplied by the same electrical potential $+u$, all the four sectors expands which results in a displacement of the actuator along the z axis (Fig. 1b lower). In the sequel, the experiments will be carried out for the x and for the y axes, the control of the z axis being similar will not be tackled. Also, we will denote U_x the voltage applied to the appropriate electrodes for the obtention of an x displacement and U_y for the y displacement.
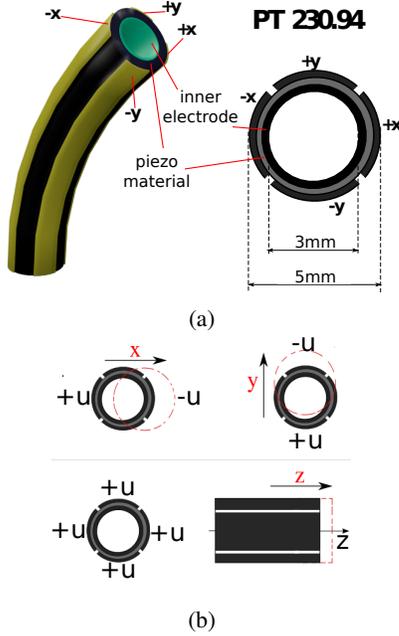

(a)

(b)

Fig. 1: Description and working principle of the piezotube. (a): perspective and top views of the PEA, (b:) working principle in order to get displacements along x, y or z.

B. The experimental setup

The experimental setup which is depicted in Fig. 2 is composed of the following elements:

- the piezotube actuator which has $27mm$ of length, $5mm$ of external diameter and $3mm$ of internal diameter. Its voltage operating range is of $\pm250V$ for a displacement range of $\pm35\mu m$ along the x axis and along the y axis. We will limit the experiments to $\pm200V$ because of the voltages amplifiers limited range.
- two optical displacement sensors which permit to measure the x and the y displacements. The sensors are the LC-2420 from *Keyence* company and are tuned to have a hundred nanometers precision and $10kHz$ of bandwidth. This bandwidth is largely enough to track certain dynamics of the actuator that permits to validate the investigated control approach.
- a computer with *Matlab/Simulink* software in order to generate the control and the reference signals, to implement the feedforward controller and to acquire the measurement.

- a dSPACE board (dS1103) that serves as DAC (digital analogic converter) and ADC (analogic digital converter) between the computer and the sensors measurement and between the computer and the actuator. The sampling frequency of the acquisition system (*Matlab-Simulink* + dSPACE board) is set to $20kHz$.
- and a voltages amplifier with two lines. It amplifies the driving voltages from the dSPACE/computer up to $\pm200V$.
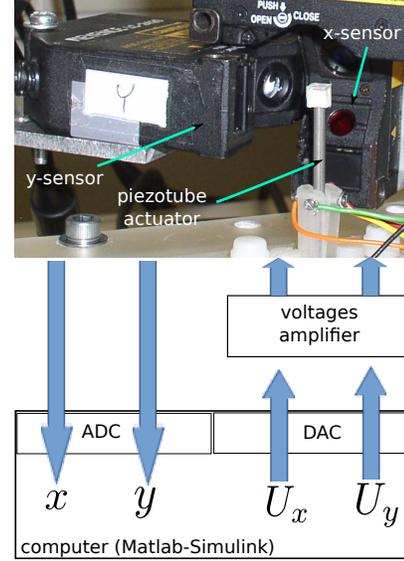

Fig. 2: Description of the experimental setup.

III. GENERAL PRINCIPLE OF THE OVERALL FEEDFORWARD CONTROL

Similar to 1-DOF piezoactuators, the piezotube actuator in this study is typified by hysteresis, creep and badly damped vibration phenomena. However additionally to them, the piezotube has strong cross-couplings. As we will observe during the characterization in the next sections, the cross-couplings are found in the hysteresis, in the creep and in the badly damped vibration at once. This makes the control strategy very challenging because we cannot anymore apply monovariable compensators as classically employed in the literature. The overall strategy is therefore as follows.

The piezotube can be considered as a system we will call S_0. Its input is the driving voltage $U = (U_x, U_y)^T$ and its output is the displacement $Y = (x, y)^T$. First, the multivariable hysteresis (i.e. hysteresis with cross-couplings) of S_0 is characterized, modeled and compensated. In order to avoid the effects of the other phenomena (creep and badly damped vibration), the hysteresis characterization and modeling are carried out with a specific driving voltage U. Afterwards, the compensator will be designed such that the hysteresis as well as related cross-couplings are reduced.

When the multivariable hysteresis compensator is implemented, a new system that we call S_H is obtained, see Fig. 3. This new system has a new driving input Y_H and is

normally typified by creep and by badly damped vibration, each one being with their own cross-couplings. The multivariable creep of this new system is therefore characterized, modeled and compensated. Thus, the piezotube S_0 augmented by the hysteresis compensator and the creep compensator yields a new system called S_L with a new driving input Y_L, see Fig. 3. Normally this new system S_L is typified by badly damped vibration only. It is also important to note that because the creep is dominant at very low frequency, the creep characterization and modeling should also be carried at very low frequency or even with constant driving input Y_H.

Finally, the badly damped vibration and cross-couplings of S_L are characterized, modeled and compensated. The presence of vibration in the actuator's response is principally due to its cantilever structure. In order to obtain a precise model of this behavior, the following types of characterization can be applied to the system S_L: harmonic, PBRS (pseudo binary random sequence), modal, or step/impulse responses approaches. Having a model from the characterization, a vibration compensation can be afterwards designed and applied. This final compensation results in a system T with input Y_R called reference or desired input. In this final system T, the hysteresis, the creep and the badly damped vibration with the cross-couplings of each are all compensated.

The complete compensator is efficient at different frequencies because of the following reasons. It compensates for the creep which is a phenomenon that occurs when the actuator is excited at very low frequency. It also compensates for the hysteresis which is a nonlinearity particularly dominant at low frequency and medium. Finally, it compensates for badly damped vibration which is a medium and high frequencies characterstics of the actuator.
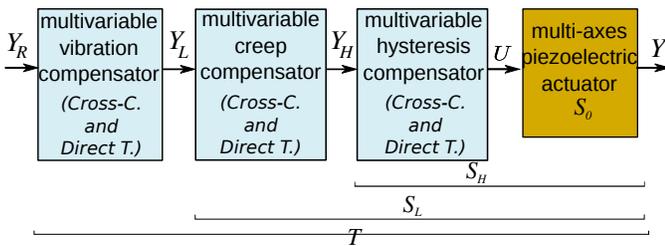

Fig. 3: Complete compensation procedure, where *Cross-C.* stands for cross-couplings and *Direct T.* stands for direct transfers.

In the next sections, the successive compensation of the different phenomena will be presented and detailed. For that, the principle scheme in Fig. 3 will be followed.

IV. CHARACTERIZATION, MODELING AND COMPENSATION OF THE MULTIVARIABLE HYSTERESIS

In this section, we consider the piezotube S_0 alone. We characterize its hysteresis and suggest a multivariable hysteresis model as well as a compensator. As we will see, a hysteresis phenomenon appears not only in the direct axis $U_x \rightarrow x$ and in the direct axis $U_y \rightarrow y$ but also in the cross-axes, i.e. in $U_x \rightarrow y$ and in $U_y \rightarrow x$. These cross-couplings also

cause loss of precision in the functioning of the piezotube and are therefore unwanted. Because the cross-couplings are also hysteresis, we will suggest a multivariable hysteresis model. On the basis of this model, the compensator will be designed to reduce the hysteresis in the direct axes and to attenuate the cross-couplings amplitudes.

A. Characterization

The hysteresis is characterized as follows. First, a sine voltage $U_x = U_a \sin(2\pi f t)$ is applied to the piezotube in order to have displacement along the x axis, the voltage U_y being left equal to zero. An amplitude of $U_a = 200$V is used. This has been chosen to correspond to the further maximal range of use. Furthermore, the hysteresis is maximal with this condition and consequently the further hysteresis model will be obtained with the worst condition. The frequency f has been chosen to be low enough in order to ensure that the dynamics does not affect the hysteresis phenomena (phase-lag effect). However, it should not be too low in order to avoid the effect of the creep on the hysteresis curve [35]. Different characterizations demonstrated that a frequency of $0.1Hz$ is a good compromise for the piezotube. The resulting displacement x is reported and the input-output map (U_x, x) is plotted in Fig. 4-a (solid line). The curve clearly shows that the x-axis of the piezotube exhibits a strong hysteresis, its amplitude being $\frac{h}{H} = \frac{10\mu m}{52\mu m} \approx 19.23\%$. In the meantime, the effect of U_x on the y axis has been observed. Fig. 4-c (solid line) depicts this effect which is also a hysteresis. The amplitude of this cross-coupling hysteresis is of about 18.8%. Much more than the cross-coupling hysteresis, the cross-coupling range itself is unwanted. Its range is of $\pm 0.55\mu m = 1.1\mu m$.

Now, the voltage U_x is set equal to zero and a sine voltage U_y is applied. Its amplitude and frequency are the same than for the x characterization above. As results, the hysteresis in the direct transfer map (U_y, y) is plotted in Fig. 4-d (solid line) which shows a hysteresis amplitude of about $\frac{10\mu m}{55\mu m} \approx 18.2\%$. The cross-coupling $U_y \rightarrow x$ which is pictured in Fig. 4-b (solid line) is also hysteretic and has a range of about $\pm 1\mu m = 2\mu m$.

B. Modeling and identification

The characterized multivariable hysteresis will be modeled in this subsection. One of the interesting hysteresis modeling approaches used in the literature is the Bouc-Wen approach. Initially developed for vibrational mechanics [54], [55], it has a very limited number of parameters making its identification straightforward and making it well adapted for real-time applications. Furthermore, its simple structure makes it very interesting in structural analysis, for instance to study the stability of a closed-loop. There are several techniques in the Bouc-Wen approach. One of them is the classical Bouc-Wen technique which can model symmetrical and rate-independent hysteresis.

The classical Bouc-Wen technique for a rectangular multivariable hysteresis (k inputs and n outputs) [48] is given by:
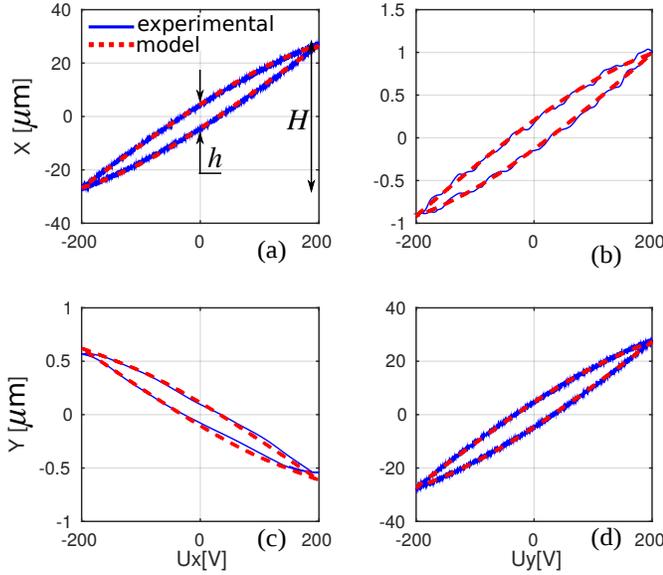
Fig. 4: Characterization (blue-solid line) and model simulation (red-dashed line) of the multivariable hysteresis.

$$\begin{cases} Y = D_p\, U - h \\ \dot{h} = A\dot{U} - B\left(|\dot{U}| \circ \hat{h}\right) - \Gamma\left(\dot{U} \circ |\hat{h}|\right), \end{cases} \quad (1)$$

where $U \in \mathbb{R}^{k\times 1}$ represents the vector of the input voltages, $Y \in \mathbb{R}^{n\times 1}$ the vector of output displacements and $h \in \mathbb{R}^{n\times 1}$ the vector of internal states of the hysteresis. D_p, A, B and Γ are matrix parameters for the multivariable classical Bouc-Wen model. In these matrices, the diagonal elements are related to the direct transfers while the rest of the elements to the cross-couplings. The operator $\circ$ denotes the Hadamard product of matrices. $\hat{U}$ and $\hat{h}$ are signals defined from U and h and depend on whether the modelled system is under or over actuated. For systems with the same number of inputs and outputs, i.e. square multivariable systems, we have $\hat{U} = U$ and $\hat{h} = h$.

From Eq.1 we derive the model of the 2-DOF piezoactuator whose characterizations are pictured in Fig. 4 (solid line):

$$\begin{cases} \begin{pmatrix} x \\ y \end{pmatrix} = \underbrace{\begin{pmatrix} D_{pxx} & D_{pxy} \\ D_{pyx} & D_{pyy} \end{pmatrix}}_{D_p} \begin{pmatrix} U_x \\ U_y \end{pmatrix} - \begin{pmatrix} h_x \\ h_y \end{pmatrix} \\[2mm] \begin{pmatrix} \dot{h_x} \\ \dot{h_y} \end{pmatrix} = \underbrace{\begin{pmatrix} A_{xx} & A_{xy} \\ A_{yx} & A_{yy} \end{pmatrix}}_{A} \begin{pmatrix} \dot{U_x} \\ \dot{U_y} \end{pmatrix} - \underbrace{\begin{pmatrix} B_{xx} & B_{xy} \\ B_{yx} & B_{yy} \end{pmatrix}}_{B} \left[\begin{pmatrix} |\dot{U_x}| \\ |\dot{U_y}| \end{pmatrix} \circ \begin{pmatrix} h_x \\ h_y \end{pmatrix} \right] \\[2mm] - \underbrace{\begin{pmatrix} \Gamma_{xx} & \Gamma_{xy} \\ \Gamma_{yx} & \Gamma_{yy} \end{pmatrix}}_{\Gamma} \left[\begin{pmatrix} \dot{U_x} \\ \dot{U_y} \end{pmatrix} \circ \begin{pmatrix} |h_x| \\ |h_y| \end{pmatrix} \right]. \end{cases} \quad (2)$$

where the elements inside D_p, A, B and Γ should be identified. Their identification is carried out by applying a nonlinear least-square optimization method that minimizes the square of the error between the discrete version of Eq.2 and the experimental data of Fig. 4 (solid line). From the identification, we obtain:

$$\begin{cases} \begin{pmatrix} x \\ y \end{pmatrix} = \underbrace{\begin{pmatrix} 0.1663 & 0.0054 \\ -0.0048 & 0.1803 \end{pmatrix}}_{D_p} \begin{pmatrix} U_x \\ U_y \end{pmatrix} - \begin{pmatrix} h_x \\ h_y \end{pmatrix} \\[2mm] \begin{pmatrix} \dot{h_x} \\ \dot{h_y} \end{pmatrix} = \underbrace{\begin{pmatrix} 0.0616 & 0.0013 \\ -0.0026 & 0.0658 \end{pmatrix}}_{A} \begin{pmatrix} \dot{U_x} \\ \dot{U_y} \end{pmatrix} - \underbrace{\begin{pmatrix} 0.0073 & 0.0002 \\ -0.0001 & 0.0054 \end{pmatrix}}_{B} \left[\begin{pmatrix} |\dot{U_x}| \\ |\dot{U_y}| \end{pmatrix} \circ \begin{pmatrix} h_x \\ h_y \end{pmatrix} \right] \\[2mm] - \underbrace{\begin{pmatrix} 0.0016 & 0.0000 \\ -0.0001 & 0.0010 \end{pmatrix}}_{\Gamma} \left[\begin{pmatrix} \dot{U_x} \\ \dot{U_y} \end{pmatrix} \circ \begin{pmatrix} |h_x| \\ |h_y| \end{pmatrix} \right]. \end{cases} \quad (3)$$

The identified model in Eq. 3 has been simulated with *Matlab-Simulink* by applying the same driving voltages than during the characterization. The simulated results are also plotted in Fig. 4 (dashed line) and conveniently fit with the experimental results.

C. Compensation

In order to reduce the hysteresis in the direct axes in Fig. 4-a and d and to render the behavior linear, we suggest to synthesize and to implement in cascade with the piezotube a hysteresis compensator. To attenuate the cross-couplings of Fig. 4-b and c at the same time, the compensator will be designed to be multivariable. For this aim, we will use the multivariable model presented in the previous subsection. Referring to Fig. 3, the hysteresis compensator should be designed in such a way that the output Y will track the compensator input Y_H, that is the compensator should satisfy:

$$Y = Y_H. \quad (4)$$

Applying this condition to the first equation of the multivariable model in Eq.1, we have:

$$Y_H = D_p\, U - h, \quad (5)$$

From Eq.5, we can derive a sufficient condition on the driving voltage U that satisfies Eq.4. We obtain:

$$U = D_p^{-1}(Y_H + h). \quad (6)$$

Eq.6 corresponds to the compensator itself which has U as output and Y_H as input, with $Y_H = (x_h, y_h)^T$. Its implementation is represented in Fig. 5 where $H(.)$ is a nonlinear operator described by the second equation of Eq.1 and is such that $h(t) = H(U)$. We can observe from this figure and from the compensator equation in Eq.6 that the direct inversion of the nonlinear part $H(.)$ is avoided, which is interesting because nonlinear inversion requires conditions that are not always possible to satisfy in the model [56], [57]. Furthermore, an extra calculation of the compensator parameters is avoided because these latters are the same than those of the initial model. This is essential especially for multivariable case where the number of parameters rapidly increases with the number of axes. We can also remark from the compensator equation and from the figure that the compensator is a rearrangement of the model. The figure shows that this rearrangement has an inverse multiplicative structure, which is similar to that

previously used for monovariable hysteresis compensation [21], [33].
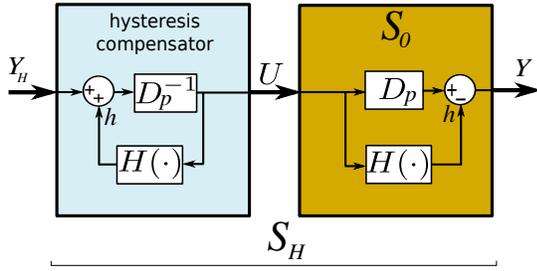

Fig. 5: Implementation of the multivariable hysteresis compensator.

The compensator of Fig. 5 was implemented and the hysteresis of the compensated system has been experimentally checked by applying sine inputs x_h and y_h with amplitude of $20\mu m$ and frequency of $0.1Hz$. The results are reported in Fig. 6. By comparing Fig. 4 and Fig. 6 we notice that the hysteresis is considerably reduced in the direct transfers (Fig. 6-a and d). The small error of compensation in these direct transfers are principally due to the fact that the hysteresis of the actuator (see Fig. 4-a and d) are non-symmetrical while the model suggested in Eq.2, and thus its compensator, is for symmetrical hysteresis only. Meanwhile, it is possible to reduce this remaining error by using the generalized Bouc-Wen model which considers non-symmetrical hysteresis [49]. On the other hand, the amplitude of the cross-couplings along the x axis has been reduced from about $\pm 1\mu m$ to about $\pm 0.55\mu m$ (Fig. 4-b and Fig. 6-b), while the amplitude of the cross-couplings along the y axis has been slightly reduced from $\pm 0.52\mu m$ to $\pm 0.47\mu m$. The compensated cross-couplings still remain nonlinear even if the hysteresis was removed. However, the main gain is the fact that their amplitudes were reduced.
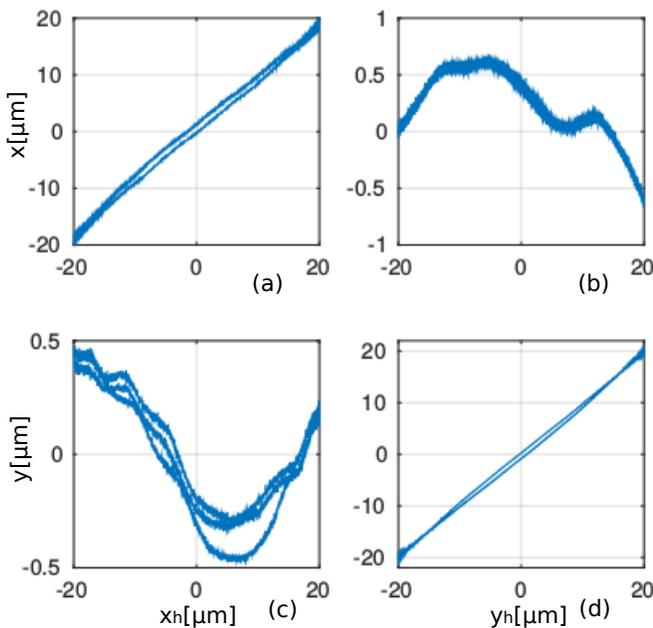
V. CHARACTERIZATION, MODELING AND COMPENSATION OF THE MULTIVARIABLE CREEP

The previous section permitted to reduce the hysteresis and to obtain a new system S_H. This new system is without hysteresis in the direct transfers. The cross-couplings are also reduced at certain condition of the input Y_H, especifically when we have Y_H a sine signal of frequency $0.1Hz$. However, the system S_H is still with creep and with badly damped vibration. In this section, we characterize, model and compensate for the creep. We will see that at the condition of creep characterization, other cross-couplings appear. The creep compensator will therefore be designed to account for these cross-couplings additionally to the creep in the direct transfers.

A. Characterization

To characterize the multivariable creep, we follow the same procedure as of the multivariable hysteresis, but we use step inputs rather than sine inputs. The creep of the system S_H is consequently studied with step inputs x_h and y_h with an amplitude of $20\mu m$. This amplitude corresponds to about the maximal range of use which is observed in Fig. 4 and Fig. 6. Notice that, from the step responses, the creep phenomenon is identified as the long duration drift that appears just after a very quick transient part. For the piezotube, Fig. 7 depict the creep of the four transfers of S_H observed during $600s$. In this, Fig. 7-a (resp. d) is the creep in the direct transfer $x_h \to x$ (resp. $y_h \to y$). On the other hand, the cross-couplings are observed in Fig. 7-b (response of x when applying a step y_h) and in Fig. 7-c (response of y when applying a step x_h). In the figures, A_f^{xx}, A_f^{xy}, A_f^{yx} and A_f^{yy} correspond to the final values of the actuator displacement before the creep occurs. They are used in the next subsection to identify the parameters of the multivariable creep model.
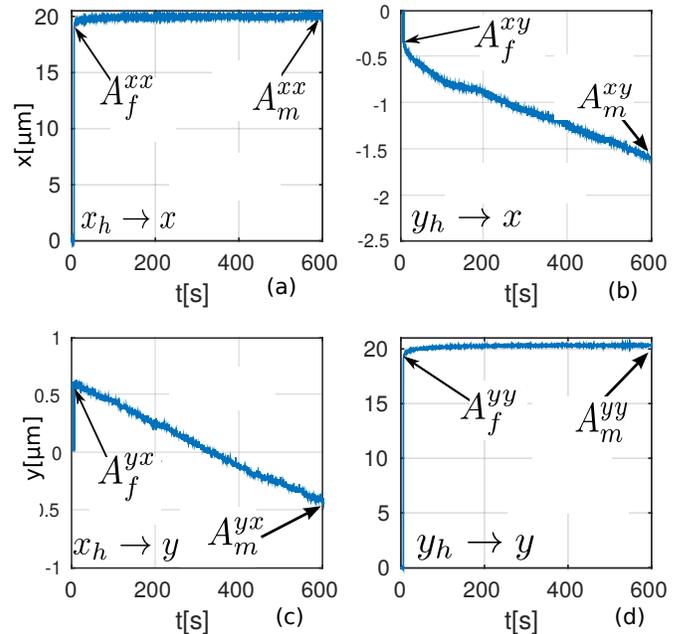

Fig. 6: Experimental results of the hysteresis compensation.

Fig. 7: Characterization of the multivariable creep.

B. Modeling and identification

Consider the direct transfer creep of Fig. 7-a which is the step response along x due to a step input x_h. This step response can be interpreted as a superposition of a constant A_f^{xx} with the drift that evolves from A_f^{xx} to A_m^{xx}. An approximation of this drift is a LTI model, as we discussed in section-I. The output x can therefore be written as follows:

$$x = [k_{xx} + C_{rxx}(s)]x_h \qquad (7)$$

where $k_{xx} = \frac{A_f^{xx}}{x_h}$ and where $C_{rxx}(s)$ is a transfer function (LTI) that describes the evolution between A_f^{xx} to A_m^{xx}.

The creeps of Fig. 7-b, c and d can also be interpreted in a similar way. This leads to the following matrix model:

$$Y = [K + C_r(s)]Y_H = KY_H + C_r(s)Y_H \qquad (8)$$

where K is a matrix gain and $C_r(s)$ is a matrix of transfer functions. Remind that the input is $Y_H = (x_h, y_h)^T$ and the output is $Y = (x, y)^T$. The detailed model is thus:

$$\underbrace{\begin{pmatrix} x \\ y \end{pmatrix}}_{Y} = \left[\underbrace{\begin{pmatrix} k_{xx} & k_{xy} \\ k_{yx} & k_{yy} \end{pmatrix}}_{K} + \underbrace{\begin{pmatrix} C_{rxx}(s) & C_{rxy}(s) \\ C_{ryx}(s) & C_{ryy}(s) \end{pmatrix}}_{Cr(s)} \right] \underbrace{\begin{pmatrix} x_h \\ y_h \end{pmatrix}}_{Y_H} \qquad (9)$$

We observe that the model Eq.8 comes back to the multi-input-multi-output creep model in [50].

The parameters of the model of Eq. 9 are identified from the experimental data of Fig. 7. The elements of the matrix parameter K are straightforward:

$$\begin{cases} k_{xx} = \frac{A_f^{xx}}{x_h} = \frac{18.91}{20} = 0.9455 \\ \\ k_{xy} = \frac{A_f^{xy}}{y_h} = \frac{-0.42}{20} = -0.0210 \\ \\ k_{yx} = \frac{A_f^{yx}}{x_h} = \frac{0.58}{20} = 0.0290 \\ \\ k_{yy} = \frac{A_f^{yy}}{y_h} = \frac{18.90}{20} = 0.9450. \end{cases} \qquad (10)$$

The procedure to identify the transfer functions of the matrix $C_r(s)$ is as follows. The experimental data related to the drift evolution from A_f^{xx} to A_m^{xx} of Fig. 7-a is separated from the whole step response curve. This drift evolution data and the step input data $x_h = 20\mu m$ are afterwards used to identify $C_{rxx}(s)$ by using the system identification Toolbox of Matlab. Here, a Box-Jenkins method was used [58]. It permits to impose the model order, to identify the parameters in an automatic manner, to verify *a posteriori* the matching level of the identified model relative to the experiment and to modify quickly the order if required. The same procedure is applied for A_f^{xy} to A_m^{xy} of Fig. 7-b, A_f^{yx} to A_m^{yx} of Fig. 7-c and for A_f^{yy} to A_m^{yy} of Fig. 7-d. We obtain the following elements of $C_r(s)$.

$$\begin{cases} C_{rxx}(s) = \frac{0.003299(s+0.01926)}{(s+0.1156)(s+0.01249)} \\ C_{rxy}(s) = \frac{-0.000484(s^2+0.004223s+6.025\times10^{-6})}{(s+0.03461)(s^2+3.9980\times10^{-7}s+1.849\times10^{-6})} \\ C_{ryx}(s) = \frac{-8.992\times10^{-5}}{s+0.0003682} \\ C_{ryy}(s) = \frac{0.00340(s+0.01996)}{(s+0.1123)(s+0.01094)} \end{cases} \qquad (11)$$

As we can see, the orders are relatively small: 1 for $C_{ryx}(s)$, 2 for $C_{rxx}(s)$ and for $C_{ryy}(s)$ and 3 for $C_{rxy}(s)$. They correspond to a minimum matching percent of 92%. In fact other tests show that when increasing the model orders, the matching percent does not anymore increase substantially. Hence the orders in Eq. 11 are a good compromise between model precision and model complexity.

The obtained LTI model $C_r(s)$ was then implemented in Matlab/Simulink, simulated and compared to the experimental data. The comparison is established in Fig. 8 where we notice that the identified model well approximates the experimental data. In this figure, only the drifts evolution is plotted and the quick jump from 0 to A_f^{ij} ($i = x, y$ and $j = x, y$) of Fig. 7 has been removed.
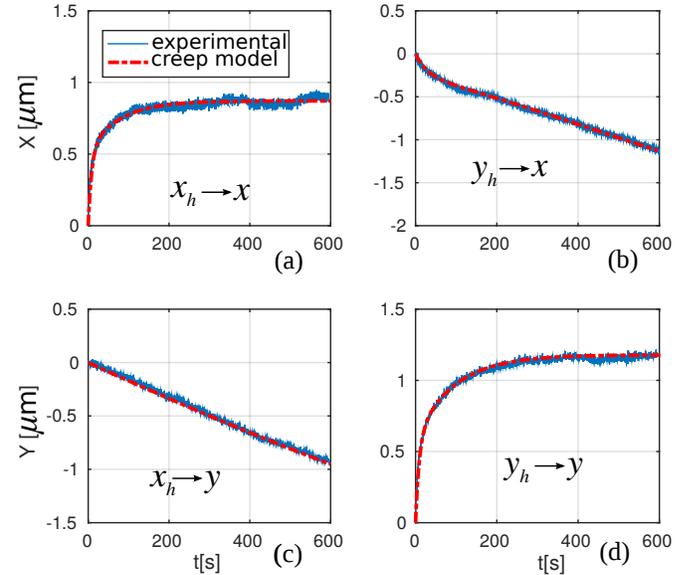

Fig. 8: Experimental data (blue-solid line) and model simulation (red-dashed line) of the multivariable creep.

C. Compensation

The compensator derivation for the creep will be similar to that for the hysteresis, which is based on the inverse multiplicative scheme. This is possible because the structure of the creep model in Eq. 8 is similar to that of the hysteresis model in the first equation of Eq. 1: the output is affine relative to the input of the system to be controlled. Let us denote $Y_L = (x_l, y_l)^T$ the creep compensator input. The output of this compensator is Y_H and this latter is the input of the system S_H to be controlled. If we desire that the output Y of S_H tracks the input Y_L, we can set $Y = Y_L$ in Eq. 8 and

derive the following sufficient condition such that this tracking condition is satisfied:

$$Y_H = K^{-1}[Y_L - C_r(s)Y_H]. \qquad (12)$$

This compensator equation has again an inverse multiplicative structure. Hence extra-calculation of the compensator parameters is avoided as they are the same than those of the model. Furthermore, dynamics direct inversion is avoided here because there is no need to invert the transfer function $C_r(s)$ which would require conditions (bistability and bicausality) that are not always satisfied during the modeling. Notice that in Eq. 12, the signal Y_H simultaneously appears in the left side and in the right side. In fact, this equation should be: $Y_H(t) = K^{-1}[Y_L(t) - C_r(s)Y_H(t - T_s)]$ where T_s is the sampling period. This means that the compensator output $Y_H(t)$ at time t is calculated on the basis of its previous value $Y_H(t - T_s)$.
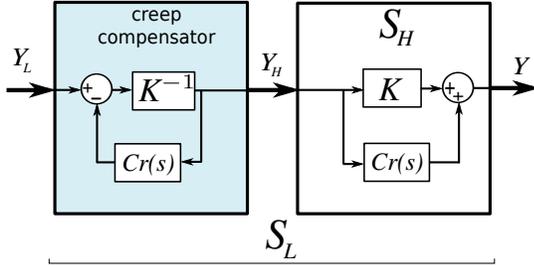

Fig. 9: Implementation of the multivariable creep compensator.

The compensator of Eq. 12 has been implemented in Matlab/Simulink following the scheme in Fig. 9 where S_H is the piezotube S_0 augmented by the hysteresis compensator as described in Fig. 5. The experimental tests consist in applying a step input $x_l = 20\mu m$ with $y_l = 0$, and then a step input $y_l = 20\mu m$ with $x_l = 0$. The responses are reported in Fig. 10 where we can see that the step responses in the direct transfers (a and d of the figure) do not anymore contain creep and where the reference value of $20\mu m$ is maintained. Furthermore, Fig. 10-b and c show that the initial cross-couplings whose evolution was given in Fig. 7-b and d have now been reduced.

VI. CHARACTERIZATION, MODELING AND COMPENSATION OF THE MULTIVARIABLE BADLY DAMPED VIBRATION

The compensation for the multivariable hysteresis and for the multivariable creep of the piezotube S_0 in the two previous sections permits to have the new system S_L with an output Y and a new input Y_L. This new system exhibits badly damped vibration when a step or an impulse input is applied. This section is dedicated to the suppression of that vibration in an open-loop fashion.

A. Characterization

To characterize the dynamics of the system S_L, an input signal Y_L that considers high frequencies should be used. This can be done with harmonic analysis which should include
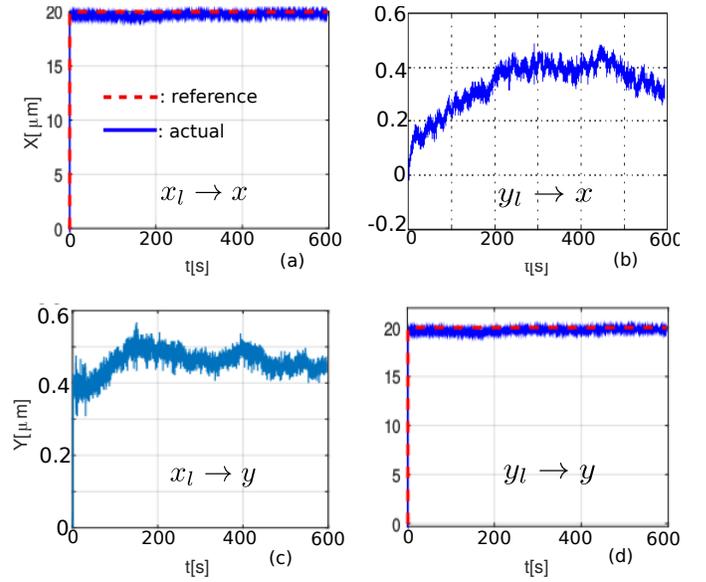

Fig. 10: Experimental results of the creep compensation.

at least the first resonant frequency, or with a pseudorandom binary sequence (PRBS) signal, or again with impulse or step signal. In this test, we will use a step input signal Y_L because of its straightforward approach: the step response is injected to a system identification technique and a model whose the order can be imposed is generated. Notice that step response approach was already used during the creep characterization, modeling and identification. Instead of using a long period of measurement ($600s$ for the creep), here, only the transient part at the begining of the step response is of interest. This transient part lasts in general less than $200ms$ for piezotube actuators due to their high bandwidth.

The experimental characterizion of the step response of S_L is represented in Fig. 11 (blue-solid line). In this, Fig. 11-a and d (blue-solid line) correspond to the response of the direct transfer $x_l \rightarrow x$ and $y_l \rightarrow y$ respectively which clearly show the vibration when applying a step input of $20\mu m$ of amplitude. On the other hand the effect of the step $x_l = 20\mu m$ to y is depicted in Fig. 11-c (blue-solid line) while the effect of the step $y_l = 20\mu m$ to x is depicted in Fig. 11-b (blue-solid line). These latter figures reveal that the cross-couplings are also typified by strong vibration.

B. Modeling

For a further compensation of the badly damped vibration, we first suggest a model for the step responses in Fig. 11 (blue-solid line). As we have removed the hysteresis and the creep, the system S_0 can be assumed to be linear. A LTI model can therefore be identified from the step reponses. We will denote $G_L(s) = YY_L^{-1}$ the (matrix) transfer function of the system S_L. It is composed of four transfer functions that link the individual inputs x_l and y_l with the individual outputs x and y.

First a transfer function $G_{Lxx}(s)$ is identified for the direct transfer $x_l \rightarrow x$. For this aim, the Box-Jenkins method of the system identification Toolbox of Matlab is again used

and applied to the experimental data of Fig. 11-a (blue-solid line). The same procedure is applied successively for the experimental data in Fig. 11-b (blue-solid line), Fig. 11-c (blue-solid line) and Fig. 11-d (blue-solid line) to yield the transfer $G_{Lxy}(s) = \frac{x}{y_l}$, $G_{Lyx}(s) = \frac{y}{x_l}$ and $G_{Lyy}(s) = \frac{y}{y_l}$ respectively. We obtain the identified model:

$$G_L(s) = \begin{pmatrix} G_{Lxx}(s) & G_{Lxy}(s) \\ G_{Lyx}(s) & G_{Lyy}(s) \end{pmatrix}. \qquad (13)$$

where

$$\begin{cases} G_{Lxx}(s) = \frac{-432.16(s-3.72e04)(s+2.707e04)(s+7853)(s+309.3)}{(s+298.2)(s^2+1.1e04s+4.449e07)(s^2+567.3s+3.783e07)} \\ \qquad \times \frac{(s^2+948.1s+5.201e07)(s^2+692.9s+1.014e08)}{(s^2+962.2s+9.867e07)(s^2+599.7s+1.051e08)}, \\ G_{Lxy}(s) = \frac{-253.1(s-4879)(s-46.75)(s^2+1568s+8.376e06)}{(s+290.8)(s^2+1417s+8.968e06)(s^2+525.8s+3.779e07)} \\ \qquad \times \frac{(s^2+4221s+6.019e07)(s^2-1454s+7.185e07)}{(s^2+678.4s+5.928e07)(s^2+898.7s+1.039e08)}, \\ G_{Lyx}(s) = \frac{-60.375(s^2+156.4s+2.038e06)(s^2+994.3s+3.495e07)}{(s+4621)(s^2+164.1s+2.03e06)(s^2+1110s+3.893e07)} \\ \qquad \times \frac{(s^2+679.5s+9.584e07)(s^2-2.06e04s+2.312e08)}{(s^2+5683s+5.045e07)(s^2+294.7s+6.392e07)}, \\ G_{Lyy}(s) = \frac{4.5368e06(s+303.8)(s^2+256.5s+6.072e07)}{(s+2.726e04)(s+5066)(s+297.3)(s^2+8639s+5.804e07)} \\ \qquad \times \frac{(s^2+83.09s+9.684e07)(s^2-4.85e04s+1.123e09)}{(s^2+468.6s+5.824e07)(s^2+167.3s+6.032e07)}. \end{cases}$$
$$(14)$$

The multivariable model in Eq. 14 has been simulated by using the step inputs x_l and y_l with amplitude 20μm. The simulation results are compared with the characterization as depicted in Fig. 11 (red dashed line), where we remark a good adequacy between them.
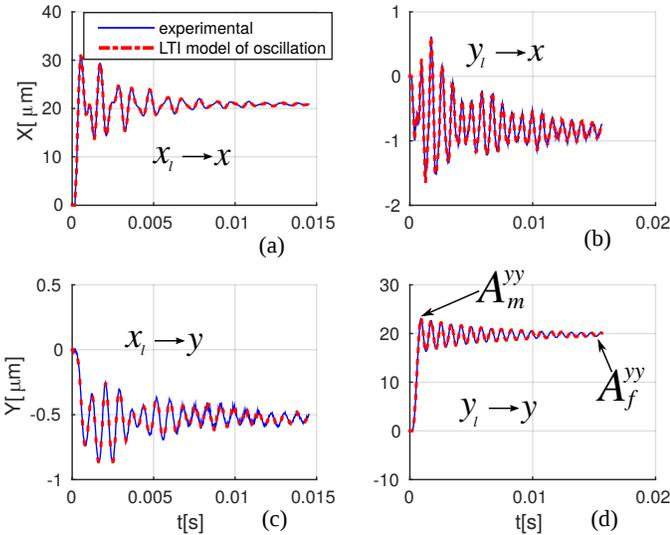

Fig. 11: Experimental characterization and model simulation of the step responses where the badly damped vibrations are illustrated.

C. Compensation

A badly damped vibration property is in general unwanted because it causes a delay in the system's response and it could also compromise the stability of the final task to be carried out. We suggest here a compensator for the badly damped vibration. Because the model Eq.14 is multivariable,

the compensator should also be multivariable in order to consider both the direct transfers and the cross-couplings.

Let Fig. 12 be the block-scheme of the system S_L with the multivariable vibration compensator $C(s)$. A new system T of output Y and input (reference) Y_R is obtained. We suggest to synthesize $C(s)$ on the basis of the standard H_∞ technique. This technique is classically employed to design feedback controller capable of accounting for the uncertainties of the model and of considering some predefined performances. Additionally to that, standard H_∞ technique can account for multivariable systems. Here, we use the technique to design the feedforward controller $C(s)$ with the possibility to consider some specified performances.
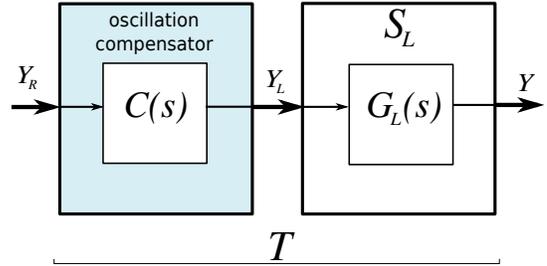

Fig. 12: Implementation of the multivariable compensator to attenuate the badly damped vibration.

In order to ease the explanation, let us first consider as if $C(s)$ and S_L were monovariable. Because the compensator $C(s)$ is designed to have an overall system $T(s)$ without vibration, let us denote $W_r(s)$ the desired behavior for this latter. The simplest behavior without vibration is a first order model. Thus let us take $W_r(s)$ as follows:

$$W_r(s) = \frac{1}{\tau s + 1} \qquad (15)$$

where τ is the time constant defined by $\tau = t_r/3$, with t_r being the desired settling time for $T(s)$. Notice that the static gain of $W_r(s)$ is set equal to one in order to ensure steady-state of Y to be equal to a constant reference Y_r.

Unfortunately the real system $T(s)$ is not in practical equal to the previous desired model $W_r(s)$. There is a dynamical model error $W_r(s) - T(s)$. A very interesting advantage of H_∞ technique is that it is also possible to give boundary for dynamical errors. For this aim, let us introduce another gain $W_1(s)$ to weight the model error $W_r(s) - T(s)$, as depicted in Fig.13. As we will see latter, the magnitude of the inverse $\frac{1}{W_1(s)}$ is a bound for the magnitude of $W_r(s) - T(s)$. Consequenly, the choice of $\frac{1}{W_1(s)}$, and thus of $W_1(s)$, can be made on the basis of specified reference tracking performances that bound the error. A possible structure for $W_1(s)$ [59] is:

$$W_1(s) = \frac{s + 3/t_r}{k_o s + 3\epsilon_s/t_r} \qquad (16)$$

where the parameter k_o is used to define the maximal allowed overshoot. For a zero vibration specification, it is set to $k_o = 1$. The parameter ϵ_s defines the tolerated static error for the compensated system. We choose 1% ($\epsilon_s = 0.01$) of

maximal static error for $W_r(s) - T(s)$, which corresponds to a specified maximal error of 1% between Y and Y_r. Finally, the specified settling time t_r is chosen to be $25ms$.

In order to moderate the driving input Y_L, we also add a weighting $W_2(s)$ as depicted in Fig.13. We will further see that the magnitude of the inverse $\frac{1}{W_2(s)}$ is a bound of the transfer $C(s) = \frac{Y_L}{Y_R}$. Thus, $\frac{1}{W_2(s)}$ can be chosen to bound the maximal driving Y_L for given Y_R. Let us take $Y_R^{\max}$ the maximal range of the reference Y_R and let us denote $Y_L^{\max}$ the maximal driving Y_L that is allowed in order to avoid the over-supply of the actuator and thus to avoid its destruction. Thus, $W_2(s)$ is chosen to be:

$$W_2(s) = \frac{Y_R^{\max}}{Y_L^{\max}} \qquad (17)$$

In the previous sections, we saw that the maximal range of voltage was $200V$ during the usage and the related displacement was of $20\mu m$. This led to a range of Y_L of $20\mu m$ and consequently a range of Y_R of the same value. Hence, the chosen weighting is.

$$W_2(s) = 1. \qquad (18)$$

The bounds and the weightings described above are for monovariable case. The piezotube in this study has two inputs and two outputs, and thus multivariable. Additionally to the desired model behavior, to the tracking performances and to the command moderation all defined by $W_r(s)$, $W_1(s)$ and $W_2(s)$ respectively, cross-couplings should also be accounted for. Consequenly, these weightings should be matrices.

Cross-couplings are unwanted phenomena that should be reduced or removed by any synthesized controller. For this aim let us choose the matricial weightings $W_r(s)$, $W_1(s)$ and $W_2(s)$ to be diagonal. By doing this structure (off-diagonal equal zero), we expect to have a controller that permits zero cross-couplings for T. Hence, from Eq.15, Eq.16 and Eq.18, and from the above discussion, we suggest:

$$\begin{cases} W_r(s) = \begin{pmatrix} \frac{1}{1 + \frac{0.025}{3}s} & 0 \\ 0 & \frac{1}{1 + \frac{0.025}{3}s} \end{pmatrix}; \\ \\ W_1(s) = \begin{pmatrix} \frac{s+120}{s+1.2} & 0 \\ 0 & \frac{s+120}{s+1.2} \end{pmatrix}; \\ \\ W_2(s) = \begin{pmatrix} 1 & 0 \\ 0 & 1 \end{pmatrix}. \end{cases} \qquad (19)$$
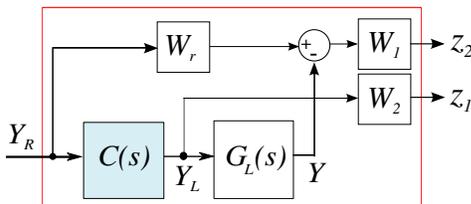

Fig. 13: The augmented controlled system.

Fig.13 is called 'augmented controlled system', as it is composed of the system $G_L(s)$ to be controlled and of the controller $C(s)$, all augmented by the weightings. It is noteworthy that the implementation and experiments will not require the weightings. These latters are only used to calculate the controller. Also the augmented controlled system has as outputs the weighted outputs z_1 and z_2 and as inputs all exogenous signal (in this case: Y_R). Referring to Fig. 13, the relation between the exogenous input Y_R and the weighted output $z = (z_1 \quad z_2)^T$ is:

$$\begin{pmatrix} z_1 \\ z_2 \end{pmatrix} = \begin{pmatrix} W_2 C \\ W_1 W_r - W_1 T \end{pmatrix} Y_R, \qquad (20)$$

where $T(s) = G_L(s)C(s)$ the transfer function of the compensated system.

Applying the standard H_∞ problem [60], the problem here consists therefore in finding the compensator $C(s)$ such that:

$$\left\| \begin{matrix} W_2 C \\ W_1 W_r - W_1 T \end{matrix} \right\|_\infty < \gamma \qquad (21)$$

By applying properties of norms, Eq. 21 is equivalent to:

$$\begin{cases} \|C\|_\infty < \|W_2^{-1}\|_\infty \gamma \\ \|W_r - T\|_\infty < \|W_1^{-1}\|_\infty \gamma \end{cases} \qquad (22)$$

where γ represents the performances evaluation parameter.

It is often more interesting in term of computation to rewrite the problem in Eq. 22 into magnitudes inequations. Hence the problem becomes in seeking the compensator $C(s)$ such that the following conditions are satisfied (which also permit to satisfy Eq. 22):

$$\begin{cases} |C| < |W_2^{-1}|\gamma \\ |W_r - T| < |W_1^{-1}|\gamma \end{cases} \qquad (23)$$

from which we can observe that the magnitude of the inverse $W_1(s)^{-1}$ is a bound for the magnitude of $W_r(s) - T(s)$ (tracking performances and model reference) and the magnitude of the inverse $W_2(s)^{-1}$ is a bound for $C(s) = Y_L Y_R^{-1}$ (command moderation), as we discussed above. If we cannot find a controller that satisfies the prescribed performances, γ will be strictly superior to one.

To solve the problem in Eq. 23, we have used the DGKF algorithm [61] and the Matlab Robust Control Toolbox. The algorithm seeks for the optimal controller and for the minimum of γ (via dichotomy iteration) that satisfy Eq. 23. After calculation, we obtain an optimal compensator $C(s)$ with an order of 34 and $\gamma = 0.9351$. We can predict that, because $\gamma < 1$, the prescribed performances will be ensured by the calculated compensator $C(s)$. In order to have a lower order compensator, we have applied a balanced realization based order reduction method to $C(s)$. The technique permitted to obtain a 12th order controller without compromising the performances.

The reduced compensator $C(s)$ has been implemented according to the scheme of Fig. 12 and reference step inputs x_r and y_r with amplitude of $20\mu m$ have been applied successively. The obtained step responses are presented in Fig.

14 where we notice the suppression of the vibration in the direct transfers and the reduction of amplitudes in the cross-couplings axes.
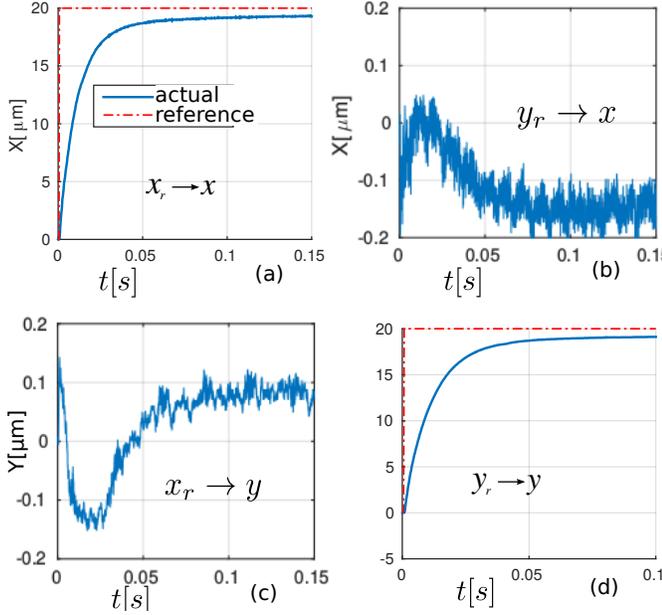

Fig. 14: Experimental results for the badly damped vibration compensation.

VII. DISCUSSIONS

A. Numerical evaluation of the compensation of hysteresis, creep, oscillations and cross-couplings

In this subsection, we discuss on the performances obtained from the designed compensator by evaluating numerically the amount of the hysteresis, of the creep, of the vibration and of the cross-couplings for each compensation procedure.

The hysteresis evaluation is made by calculating the amplitude $\frac{h}{H}$ for the non-compensated hysteresis in Fig. 4 and for the compensated hysteresis in Fig. 6. To evaluate the creep and its compensation, we refer to Fig. 7 and Fig. 10. Finally the vibration is quantified by calculating the step responses overshoots in Fig. 11 and Fig. 14. More precisely, the creep and the vibration are quantified by using the ratio $[(A_m - A_f)/A_f] \times 100\%$. For the creep, A_m and A_f refer to the displacement before the creep appears and the displacement after the time for the creep evaluation, as depicted in Fig. 7. For the vibration, A_m and A_f stand for the maximal displacement observed on the step response, i.e. the overshoot, and the displacement after the settling time, i.e. the final value (see Fig. 11a). The quantitative evaluation is made for the direct transfers. Tab. I rassembles the data. It clearly shows that the maximal hysteresis of 19.23% amplitude was reduced to about 0.01%, the maximal creep was reduced from 5.5% to about 0.04% and the maximal overshoots for the two axes were removed completely.

To evaluate the efficiency of the complete compensator (the three individual compensators in cascade) to reduce the cross-couplings, we now calculate the cross-couplings without

TABLE I: Numerical evaluation of the hysteresis, of the creep and of the vibration (for direct transfers).

	Before compensation			After compensation		
	Hyst.	Creep	Oscil.	Hyst.	Creep	Oscil.
X	19.23%	4.6%	45.1%	0.01%	0.31%	0.00%
Y	18.2%	5.5%	15.6%	0.01%	0.04%	0.00%

compensation from Fig. 4 and those after the whole compensation from Fig. 14. For example, to quantify the cross-coupling along x axis, we consider the residual displacement denoted H^{xy} in x when an input along y is applied. From this, the cross-coupling amplitude is the ratio between this residual displacement H^{xy} face to H^{xx}, this latter being the displacement when an input is applied in the same x axis. This definition indicates the relative affordability of the x axis to be affected by the y axis, as is used in [62]. The same definition is applicable for the cross-coupling in the y axis. Tab. II rassembles the results and shows that the complete compensator has lowered the cross-couplings amplitudes from a maximal value of 3.1% to about 0.5%.

TABLE II: Cross-couplings amplitudes before and after the complete compensation.

	Initial system (S_0)	Completely compensated system (T)
X	$\frac{H^{xy}}{H^{xx}} = \frac{1.8}{56.5} = 3.1\%$	$\frac{A_f^{xy}}{A_f^{xx}} = \frac{0.11}{19} = 0.5\%$
Y	$\frac{H^{yx}}{H^{yy}} = \frac{1.1}{55.2} = 1.9\%$	$\frac{A_f^{yx}}{A_f^{yy}} = \frac{0.1}{19} = 0.5\%$

B. Complex trajectory tracking

In order to test the capability of the controlled actuator to track complex trajectory, we use a spatial circular reference input obtained by applying two shifted sine references x_r and y_r. First we choose a radius of $20\mu m$ for the circle. Fig.15a depicts the results. The figure also depicts the (scaled) output trajectory when there is no compensation. From them, we can see that the output trajectory obtained when using the complete compensation tracks the reference trajectory much better than when there is no compensation. Fig.15b depicts the results when using a radius of $30\mu m$, additionally to those with a radius of $20\mu m$. These results show that the complete compensation technique permits to have more regular output trajectory and allows a much better tracking of the reference.
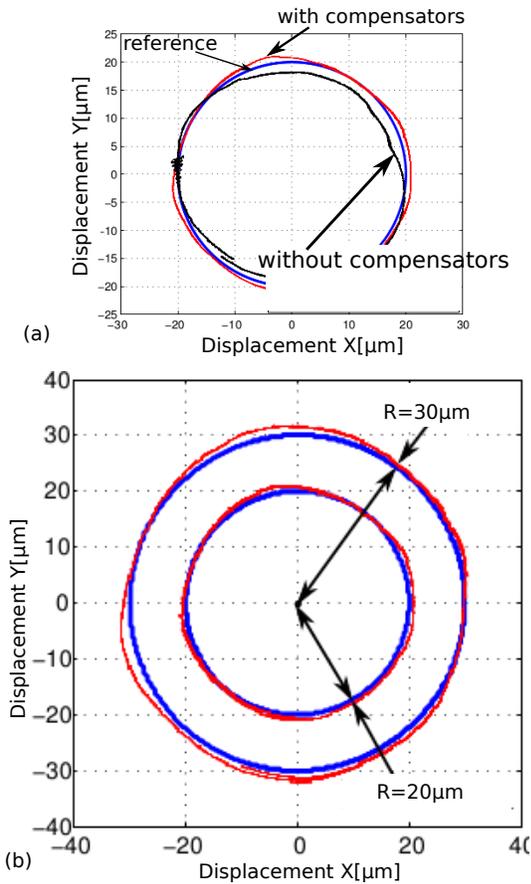
Fig. 15: Circular trajectory tracking.

C. Commutativity of the compensators

In this paper, the principle of the complete compensation of the hysteresis, creep, badly damped vibration and cross-couplings is schemated in Fig. 3. First the hysteresis and related cross-couplings were compensated for; then the creep and related cross-couplings, and finally the vibration and related cross-couplings. In fact each step corresponds to a range of frequency: low frequency for the hysteresis, very low frequency for the creep, and medium and high frequency for the vibration. Consequently, each individual compensator is valuable for the reduction or cancelling of each phenomenon in the related range of frequency. Since each compensator is multivariable, the cross-couplings found in each range of frequency are also removed. As a result, the cascade of the three individual compensators permits to cover the different phenomena in a wide range of frequency.

It is also possible to commute the individual compensators, rather than following the scheme in Fig. 3. By doing so, the identification steps should also be adapted accordingly. Let us consider for example the complete compensation in Fig. 16. To apply this scheme, the creep is first characterized and identified from the piezotube S_0. After implementation of the creep compensator, a new system S_a of input Y_a is obtained. Then, to compensate for the badly damped vibration of S_a, the dynamics should be characterized and modeled from this latter system. The implementation of the vibration compensator results in a new system S_b with a new input Y_b. Finally, the

hysteresis is characterized, modeled and compensated for from S_b. The complete compensation in this case gives a system T that is similar to that of Fig. 3. Furthermore, the cross-couplings are also accounted for in this case as long as each individual compensator is multivariable.
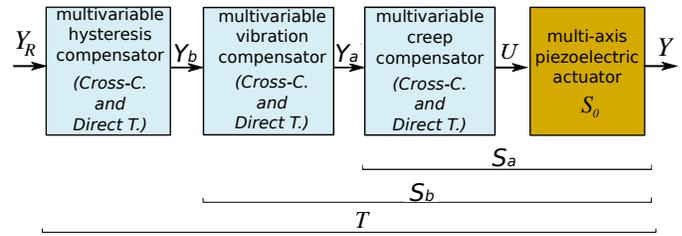

Fig. 16: Complete compensation with a different scheme than that of Fig. 3 and where *Cross-T.* stands for cross-couplings and *Direct-T.* stands for direct transfers.

D. Other remarks

A main limitation of feedforward control is the lack of robustness against external disturbances and against model uncertainties. The complete compensation technique developed in this paper does not avoid this rule. For instance, a temperature variation in the ambient environment could reduce the efficiency of the complete compensation. One interesting approach to tackle this example consists in placing a temperature sensor (which is embeddable) onto the actuator or in its vicinity. The information from this sensor can then be used to automatically sequence the parameters of the three compensators (of hysteresis, of creep and of vibration) such that they become adaptive. This adaptive and temperature-dependent compensation is possible at the cost of a thorough and precise analysis and modeling of the phenomena to be compensated for. Indeed the derivation of the temperature-dependent compensators requires a precise temperature-dependent model.

Applications such as SPM and AFM based images scanning might require to drive the piezoactuator at high frequency. At such frequency, the creep and the hysteresis effects are less dominant than the dynamics of the actuator and than the vibration phenomenon. The weightings in Eq.19 are therefore the principal parameters to be tuned in order to increase the bandwidths of the final compensated system. Different tests shown however that there is a limitation in this tuning. In fact, increasing the bandwidths decreases the damping performances. A compromise should be found. In the numerical example given in Eq.19, the specified bandwidth was equal to $120Hz$ (corresponding to the specified settling time of $t_r = 25ms$) which provided a completely damped vibration.

VIII. CONCLUSIONS

This paper suggested the complete control of the hysteresis, of the creep and of the badly damped vibration in a 2-DOF piezotube actuator without using feedback sensors. The principle consisted in cascading the individual compensators of each phenomenon and in using them as feedforward controllers. First, the hysteresis was characterized, modeled and

compensated for; then the creep and finally the badly damped vibration. Each step was based on a multivariable modeling and compensation permitting to consider and then to attenuate the cross-couplings. Experimental tests were carried out to validate each step and demonstrated the efficiency of the approach. The hysteresis which could initially exceed 19% was reduced to about 0.01% while the creep was reduced from 5.5% to 0.04%. Regarding the vibration, related overshoots that could exceed 45% were completely removed.

ACKNOWLEDGMENT

REFERENCES

[1] S. Devasia, E. Eleftheriou and SOR Moheimani, "A survey of Control Issues in Nanopositioning", IEEE Transactions on Control Systems Technology, Vol.15, pp.802-823, 2007.

[2] M. Rakotondrabe, K. Rabenorosoa, J. Agnus and N. Chaillet, " Robust Feedforward-Feedback Control of a Nonlinear and Oscillating 2-DOF Piezocantilever", IEEE Transactions Automation Science and Engineering, Vol.8, pp.506–519, 2011

[3] A. Bazaei, Y.K. Yong, SOR Moheimani and A. Sebastian, "Tracking of Triangular References Using Signal Transformation for Control of a Novel AFM Scanner Stage",IEEE Transactions on Control Systems Technology, pp. 453-464, 2012

[4] M. Rakotondrabe, Y. Haddab and P. Lutz, 'Plurilinear modeling and discrete μ-synthesis control of a hysteretic and creeped unimorph piezoelectric cantilever', IEEE Int Conf Automation, Robotics, Control and Vision), pp:57-64, Grand Hyatt Singapour, December 2006.

[5] S. Salapaka, A. Sebastian, J.P. Cleveland and M. Salapaka, "High bandwidth nano-positioner: A robust control approach", Review of scientific instruments, Vol.73, pp.3232–3241, 2002

[6] N. Tamer and M. Dahleh, "Feedback control of piezoelectric tube scanners", IEEE Conference on Decision and Control, pp.1826–1831, 1994

[7] A.J. Fleming and K.K. Leang, "Integrated strain and force feedback for high-performance control of piezoelectric actuators", Sensors and Actuators A: Physical, Vol.161, pp.256–265, 2010

[8] J.A. Escareno, M. Rakotondrabe and D. Habineza, 'Backstepping-based robust-adaptive control of a nonlinear 2-DOF piezoactuator', IFAC Control Engineering Practice (CEP), Vol.41, Pages 57-71, August 2015.

[9] M. Rakotondrabe and Y. Le Gorrec, 'Force control in piezoelectric microactuators using self scheduled H_∞ technique', IFAC Symposium on Mechatronic Systems, pp.417:422, Cambridge Massachusetts USA, September 2010.

[10] M. Rakotondrabe, 'Smart materials-based actuators at the micro/nano-scale: characterization, control and applications', edited book, Springer Verlag, New York, ISBN 978-1-4614-6683-3, 2013.

[11] J. Dosch, D. Inman, and E. Garcia,'A Self-Sensing Piezoelectric Actuator for Collocated Control', Journal of intellgint Matterials and smart structuctures, vol.166(3), 1992.

[12] A. S. Putra, H. Sunan, T. K. kok, S. K. Panda and T. H. Lee, 'Self-sensing actuation with adaptive control switching trajectory', IEEE/ASME Transactions on Mechatronics, vol.13(7), 2008.

[13] P. C. Khiang, G. Guoxiao, M. B. Chen, and T. H. Lee, 'Self-Sensing Actuation for Nanopositioning and Active-Mode Damping in Dual-Stage HDDs', IEEE/ASME Transactions on Mechatronics, 11, 2006.

[14] T. Rittenschober and K. Schlacher, 'Observer-based self sensing actuation of piezoelastic structures for robust vibration control' Automatica, 48, 1123-1131, 2012.

[15] H. Ikeda and T. morita, 'High-precision positioning using a self-sensing piezoelectric actuator control with a differential detection method', Sensors and Actuators A: Physical, 170, 147-155, 2011.

[16] S. Kuiper and G. Schitter, 'Active damping of a piezoelectric tube scanner using self-sensing piezo actuation', Mechatronics, 20, 656-665, 2010.

[17] A.J. Fleming and S.O.R. Moheimani, 'Sensorless Vibration Suppression and Scan Compensation for Piezoelectric Tube Nanopositioners' IEEE/ASME Trans on Mechatronics, 14(1), 2006.

[18] I.A. Ivan, O. Aljanaideh, J. Agnus, P. Lutz and M. Rakotondrabe, 'Quasi-static displacement self-sensing measurement for a 2-DOF piezoelectric cantilevered actuator', IEEE Transactions on Industrial Electronics (TIE), DOI.10.1109/TIE.2017.2677304, 2017.

[19] M. Rakotondrabe, 'Combining self-sensing with an Unkown-Input-Observer to estimate the displacement, the force and the state in piezoelectric cantilevered actuator', ACC, (American Control Conference), pp.4523-4530, Washington DC USA, June 2013.

[20] K. Klaus and H. Janocha,"Inverse feedforward controller for complex hysteretic nonlinearities in smart-material systems", Control Intelligent Systems, Vol.29, pp.74–83, 2001

[21] M. Rakotondrabe, "Classical Prandtl-Ishlinskii modeling and inverse multiplicative structure to compensate hysteresis in piezoactuators", American Control Conference, Vol.10, pp.1646-1651 , 2012

[22] ———, 'Multivariable classical Prandtl-Ishlinskii hysteresis modeling and compensation and sensorless control of a nonlinear 2-dof piezoactuator', Springer Nonlinear Dynamics, DOI: 10.1007/s11071-017-3466-5, March 2017

[23] M. Al Janaideh, M. Rakotondrabe and O. Al Janaideh 'Further Results on Hysteresis Compensation of Smart Micro-Positioning Systems with the Inverse Prandtl-Ishlinskii Compensator, IEEE Transactions on Control Systems Technology, doi:10.1109/TCST.2015.2446959.

[24] W.T. Ang, WP. Khosla, C.N. Riviere, "Feedforward controller with inverse rate-dependent model for piezoelectric actuators in trajectory-tracking applications", Transactions on Mechatronics, IEEE/ASME, Vol.12, pp.134–142, 2007

[25] O. Aljanaideh, M. Al Janaideh and M. Rakotondrabe, 'Enhancement of Micro-positioning Accuracy of a Piezoelectric Positioner by Suppressing the Rate-Dependant Hysteresis Nonlinearities', IEEE/ASME Intern Conf on Advanced Intelligent Mechatronics), pp.1683-1688, BesanÃğon, France, July 2014

[26] H. Jiang, H. Ji, J. Qiu, Y. Chen, Yuansheng," A modified prandtl-ishlinskii model for modeling asymmetric hysteresis of piezoelectric actuators", Ultrasonics, Ferroelectrics and Frequency Control, IEEE Transactions on, pp. 1200–1210, 2010

[27] O. Al Janaideh, M. Al Janaideh and M. Rakotondrabe, 'Inversion-free feedforward dynamic compensation of hysteresis nonlinearities in piezoelectric micro/nano-positioning actuators', IEEE Int Conf on Robotics and Automation), pp.2673-2678, Seattle Washington USA, May 2015.

[28] G. Song, J. Zhao, X. Zhou, et al, "Tracking control of a piezoceramic actuator with hysteresis compensation using inverse Preisach model", Mechatronics, IEEE/ASME Transactions on, Vol.10, pp.198–209, 2005

[29] H. Hu, B. Mrad, "On the classical Preisach model for hysteresis in piezoceramic actuators", Mechatronics, Vol.13, pp.85–94, 2002

[30] P. Ge, M. Jouaneh, "Generalized Preisach model for hysteresis nonlinearity of piezoceramic actuators", Precision Engineering, Vol.20, pp.99–111, 1997

[31] R. V. Iyer, X. Tan, P. S. Krishnaprasad, " Approximate inversion of the Preisach hysteresis operator with application to control of smart actuators", IEEE Transactions on Automatic Control, vol. 50, no. 6, pp. 798-810, 2005

[32] R. Oubellil, L. Ryba, A. Voda, M. Rakotondrabe, 'Experimental model inverse-based hysteresis compensation on a piezoelectric actuator', IEEE ICSTCC, (International Conference on System Theory, Control and Computing), pp.186-191, Cheile Gradistei - Fundata Resort, Romania, October 2015.

[33] M. Rakotondrabe, "Bouc-Wen modeling and inverse multiplicative structure to compensate hysteresis nonlinearity in piezoelectric actuators", IEEE Transactions on Automation Science and Engineering, Vol.8, pp.428-431, 2011

[34] H. Jung, J.Y. Shim and D. Gweon, "New open-loop actuating method of piezoelectric actuators for removing hysteresis and creep", Review of Scientific Instruments, 71 (9), pp.3436-3440, 2000.

[35] M. Rakotondrabe, 'Modeling and Compensation of Multivariable Creep in multi-DOF Piezoelectric Actuators', IEEE Int.. Conference on Robotics and Automation, pp.4577-4581, St Paul Minnesota USA, May 2012.

[36] M. Rakotondrabe, 'Piezoelectric systems for precise and high dynamic positioning: design, modeling, estimation and control', HDR halititation thesis, University of Franche-Comté / FEMTO-ST, November 10, 2014.

[37] M. Rakotondrabe, K. Rabenorosoa, J. Agnus and N. Chaillet, 'Robust feedforward-feedback control of a nonlinear and oscillating 2-dof piezocantilever', IEEE Transactions on Automation Science and Engineering,V ol.8, Issue.3, pp.506-519, July 2011.

[38] G. Schitter, A. Stemmer, F. Allgower, âĂİRobust 2 DOF-control of a piezoelectric tube scanner for high speed atomic force microscopyâĂİ, American Control Conference, pp. 3720âĂŞ3725, June 2003.

[39] H. Jung, J. Youp Shim and D. Gweon, 'Tracking control of piezoelectric actuators', Nanotechnology 12, 14-2, 2001.

[40] B. Mokaberi and A. A. G. Requicha, "Compensation of scanner creep and hysteresis for AFM nanomanipulation", IEEE Transactions on Automation Science and Engineering, pp.197-208, 2008.

[41] M. Rakotondrabe, C. Clevy and P. Lutz, 'Hysteresis and vibration compensation in a nonlinear unimorph piezocantilever', IEEE/RSJ International Conference on Intelligent Robots and Systems, pp:558-563, Nice France, Sept 2008.

[42] D. Croft, G. Shed, and S. Devasia, 'Creep, hysteresis and vibration compensation for piezoactuators: atomic force microscopy application', ASME Journal of Dynamic Systems, Measurement and Control, 2001.

[43] M. Rakotondrabe, 'Smart materials-based actuators at the micro/nano-scale: characterization, control and applications', edited book, Springer - Verlag, New York, ISBN 978-1-4614-6683-3, 2013.

[44] M. Rakotondrabe, J. Agnus, P. Lutz, "Feedforward and IMC-feedback control of a nonlinear 2-DOF piezoactuator dedicated to automated tasks", IEEE Conference on Automation Science and Engineering, pp.393–398, 2011

[45] H. Habibullah, H.R. Pota, I.R. Petersen and M.S. Rana, "Reduction of cross-coupling between X-Y axes of piezoelectric scanner stage of atomic force microscope for faster scanning," Control Applications (CCA), 2013 IEEE International Conference on , pp.455–460, 2013

[46] I. Mahmood, K. Liu, SOR Moheimani, "Two sensor based hinf control of a piezoelectric tube scanner", IFAC World Congress, pp.8251–8256, 2008

[47] Y. Al Hamidi and M. Rakotondrabe, 'Feedforward and output feedback control of a highly oscillating and nonlinear 2-DOF piezoelectric actuator by using input shaping compensator and a linear quadratic regulator', SPIE Sensing Technology+Applications; Sensors for Next Generation Robots conference , doi:10.1117/12.2229008, Baltimore Maryland USA, April 2016.

[48] D. Habineza, M. Rakotondrabe , and Y. Le Gorrec, "Bouc-Wen modeling and feedforward control of multivariable hysteresis in piezoelectric systems: application to a 3-DoF piezotube scanner," IEEE Trans. Control Syst. Technol., Vol. 23, No. 5, pp. 1797–1806, 2015.

[49] D. Habineza, M. Rakotondrabe and Y. Le Gorrec, 'Multivariable generalized Bouc-Wen modeling, identification and feedforward control and its application to a 2-DoF piezoelectric multimorph actuator', IFAC World Congress, pp.10952-10958, Cape Town, South Africa, August 2014.

[50] M. Rakotondrabe, "Modeling and compensation of multivariable creep in multi-DOF piezoelectric actuators," IEEE Int. Conf. Robot. Automation, St Paul MN, USA, pp. 4577âĂŞ4581, 2012.

[51] D. Habineza, M. Rakotondrabe and Y. Le Gorrec, ' Simultaneous Suppression of Badly-Damped Vibrations and Cross-couplings in a 2-DoF piezoelectric actuator, by using Feedforward Standard H-inf approach', SPIE Sensing Technology+Applications; Sensors for Next Generation Robots conference , 9494-29, Baltimore Maryland USA, April 2015.

[52] Y. Al Hamidi and M. Rakotondrabe, 'Multi-Mode Vibration Suppression in 2-DOF Piezoelectric Systems Using Zero Placement Input Shaping Technique', SPIE Sensing Technology+Applications; Sensors for Next Generation Robots conference , 9494-27, Baltimore Maryland USA, April 2015.

[53] Y. Al Hamidi and M. Rakotondrabe , 'Multi-Mode Vibration Suppression in a multi-DOF Piezoelectric Tube Actuator by extending the Zero Placement Input Shaping Technique', MDPI Actuators, 5(2), 13, doi:10.3390/act5020013, April, 2016.

[54] R. Bouc, "Forced vibration of mechanical systems with hysteresis", Conference on Nonlinear Oscillation, Prague, 1967.

[55] Y. K. Wen, "Method for random vibration of hysteresis systems", Journal of the Engineering Mechanics Division, vol. 102, pp. 249-263, 1976.

[56] O. Al Janaideh , M. Rakotondrabe, H. Khasawneh and M. Al Janaideh, 'Rate-dependent Prandtl-Ishlinskii hysteresis compensation using inverse-multiplicative feedforward control in magnetostrictive Terfenol-D based actuators', American Control Conference, pp.649-654, Boston MA USA, July 2016.

[57] O. Aljanaideh, D. Habineza, M. Rakotondrabe and M. Al Janaideh, 'Experimental comparison of rate-dependent hysteresis models in characterizing and compensating hysteresis of piezoelectric tube actuators, Elsevier Physica B: Condensed Matter (Physica B), doi:10.1016/j.physb.2015.10.021, oct 2015.

[58] L. Ljung, "System identification toolbox", The matlab user's guide.

[59] S. Khadraoui, M. Rakotondrabe and P. Lutz, 'Combining H-inf approach and interval tools to design a low order and robust controller for systems with parametric uncertainties: application to piezoelectric actuators', International Journal of Control, vol. 85, no1-3, pp. 251-259, 2012.

[60] K. Zhou, J. C. Doyle and K. Glover, 'Robust and optimal control', Prentice-Hall, Englewood Cliffs, ISBN-13: 978-0134565675, 1995.

[61] J. C. Doyle, K. Glover, P. K. Khargonekar and B. A. Francis, 'State-space solutions to standard H2 and Hinf control problems', IEEE Transactions on Automatic Control, vol. 34, no. 8, pp.831–846, 1989.

[62] M. Rakotondrabe, A. Fowler and S.O.R. Moheimani, 'Control of a novel 2-DoF MEMS nanopositioner with electrothermal actuation and sensing', IEEE Transactions on Control Systems Technology, 22(4), Page 1486-1497, July 2014.

Didace Habineza received the Engineer diploma in Electrical Engineering from Ex-American Institute of Boumerdes University (Algeria) in 2010 and his MSc in Mechatronics from the Université de Franche Comté (France) in 2012. He obtained the PhD degree from the Université Bourgogne Franche-Comté with research affiliation at the FEMTO-ST research institute in 2015. His PhD works focused on feedforward control of multi-axes piezoelectric systems. He is now engineer at HTi Automotive counsulting.

Mahmoud Zouari obtained the national engineering diploma in Mechatronics from the Ecole Supérieure de Technologie et d'Informatique in Tunisia in 2013 and the MSc on Mechatronics from the UniversitÃľ de Franche-Comté, France, in 2015. He was internship at the department of Automatic Control and MicroMechatronic Systems department of FEMTO-ST in 2015.
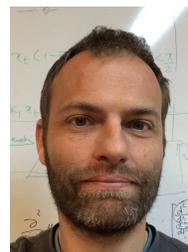
Yann Le Gorrec was graduated as engineer in "Control, Electronics, Computer Engineering" at the National Institute of Applied Sciences (INSA, Toulouse, France) in 1995. He received in 1998 his Ph. D. degree from the National Higher School of Aeronautics and Aerospace (Supaero, Toulouse, France). His field of interest was robust control and self scheduled controller synthesis. From 1999 to 2008, he was Associate Professor in Automatic Control at the Laboratory of Control and Chemical Engineering of Lyon Claude Bernard University (LAGEP, Villeurbanne, France). He worked on port Hamiltonian systems and their use for the modeling and control of irreversible and distributed parameter systems with an application to physico-chemical processes. From september 2008 he is Professor at National Engineering Institute in Mechanics and Microtechnologies. His current field of research is the control of non linear systems and infinite dimensional systems with an application to smart material based actuators, and micro actuators.

Micky Rakotondrabe (S'05, M'07) is Associate Professor at the Université de Franche-Comté since 2007 with research affiliation at the AS2M department of FEMTO-ST institute. He obtained the HDR in control systems in 2014. He was leader of the CODE group ("Control & Design") group at FEMTO-ST from 2015 to 2017. Since 2017, he founded the MACS group (Methodologies for Automatic Control and for Design of Mechatronic Systems). He is also head of the international master on Control for Green Mechatronics (GREEM) of the Université Bourgogne Franche-Comté, all in France.

Micky Rakotondrabe is or was associate or guest editor in prestigious journals related to Automation and Mechatronics or to Micro Nano (IEEE/ASME Trans Mechatronics, IFAC Mechatronics, IEEE Robotics Automation Letter, MDPI Actuators) and member of two Technical Committees related to the same fields (IEEE/RAS TC on Micro/Nano Robotics and Automation, IFAC TC on mechatronics). He received several recognition prizes. In 2016, he is recipient of the Big-On-Small award delivered during the IEEE MARSS international conference. This award is to recognize a young professional (<40yo) with excellent performance and international visibility in the topics of mechatronics and automation for manipulation at small scales.